UNIVERSITY of CALIFORNIA
SANTA CRUZ

ELLIPSOIDAL ALGORITHM FOR FAST COMPUTATION OF REACHABLE TUBES

A thesis submitted in partial satisfaction of the
requirements for the degree of

MASTER OF SCIENCE

in

SCIENTIFIC COMPUTING AND APPLIED MATHEMATICS

by

Lia M. Gianfortone

September 2018

The thesis of Lia M. Gianfortone is approved:

Professor Abhishek Halder

Professor Hongyun Wang

Professor Qi Gong

Lori Kletzer
Vice Provost, Dean of Graduate Studies

Contents

Abstract

Ellipsoidal Algorithm for Fast Computation of Reachable Tubes

by

Lia M. Gianfortone

We study the problem of computing the forward "reachable tube", defined as a temporal union of the "reach sets" of a dynamical system, or the sets of states the system can attain in future instances of time when subject to set-valued uncertainties in its initial conditions, controls, and exogenous disturbances. Fast computation of the reachable tubes for uncertain dynamical systems is essential for safety-critical applications such as autonomous driving and unmanned aerial systems traffic management where much of the high-level decision making (e.g., lane changing in autonomous driving or switching between motion primitives during flight of an unmanned aerial system) critically depends on the reachable tubes. At the same time, computation of the reachable tubes is difficult in general, due to the high-dimensional, non-convex nature of the problem. Yet applications mentioned before demand their accurate computation at a time scale much smaller than that of the physical dynamics.

In this thesis, we propose a framework for computing tight outer approximations of forward reachable tubes in real-time that leverages parallel computation. Our algorithm builds on ellipsoidal calculus and convex optimization. We report numerical results to demonstrate the efficacy of the proposed algorithm.

1

Introduction

1.1 Motivation and Overview

Verification of motion under uncertain conditions is necessary for many applications, e.g., trajectory planning and collision avoidance for unmanned vehicles such as drones or self-driving cars operating in dynamic environments. Verification is non-trivial task because all possible states that a system can reach must be accounted for, and the underlying dynamics may have high-dimensional state space. Thus, simulating a large but finite number of trajectories (as in Monte Carlo) does not lead to provable verification.

Reachability analysis provides approaches for provable verification that involves computing the so-called *reach sets* for set-valued uncertainties in initial state vector $\boldsymbol{x}_0$, controls $\boldsymbol{u}(t)$, and exogenous disturbances $\boldsymbol{w}(t)$. At time t, let the dynamical system of interest have state vector $\boldsymbol{x}(t) \in \mathbb{R}^n$, the controls $\boldsymbol{u}(t) \in \mathcal{U}(t) \subset \mathbb{R}^m$, and

the disturbances $\boldsymbol{w}(t) \in \mathcal{W}(t) \subset \mathbb{R}^d$. We assume that the sets $\mathcal{U}(t), \mathcal{W}(t)$ are compact for all $t \geq t_0$. The reach set at time t, denoted as $\mathcal{X}[t] \coloneqq \mathcal{X}(t, t_0, \boldsymbol{x}_0) \subset \mathbb{R}^n$ is the set of all state vectors $\boldsymbol{x} \coloneqq \boldsymbol{x}\,(t, t_0, \boldsymbol{x}_0)$ that can be realized at time t starting from the initial condition $\{t_0,\ \boldsymbol{x}_0\}$, where $\boldsymbol{x}_0 \coloneqq \boldsymbol{x}(t_0)$. Succinctly,

$$\mathcal{X}(t, t_0, \boldsymbol{x}_0) = \bigcup_{\substack{\boldsymbol{u}(t)\in\mathcal{U}(t),\\ \boldsymbol{w}(t)\in\mathcal{W}(t)}} \boldsymbol{x}(t, t_0, \boldsymbol{x}_0) \tag{1.1}$$

For a set-valued initial state, $\mathcal{X}_0 \subset \mathbb{R}^n$, the reach set at time t resulting from $\{t_0, \mathcal{X}_0\}$ is

$$\mathcal{X}(t, t_0, \mathcal{X}_0) = \bigcup_{\boldsymbol{x_0}\in\mathcal{X}_0} \mathcal{X}(t, t_0, \boldsymbol{x}_0) \tag{1.2}$$

The *reachable tube* $\widetilde{\mathcal{X}}(t, t_0, \mathcal{X}_0)$ for the interval $[t_0, t]$ is the $(n+1)$-dimensional set generated by the time unions of the reach sets within that interval, that is,

$$\widetilde{\mathcal{X}}(t, t_0, \mathcal{X}_0) = \bigcup_{t_0\leq\tau\leq t} \mathcal{X}(\tau, t_0, \mathcal{X}_0). \tag{1.3}$$

The sets $\mathcal{X}$ and $\widetilde{X}$ generated by an uncertain dynamical of a system can be checked against the sets of desirable and undesirable states to verify safety [17]. Discretizing the sets of initial conditions, controls, and disturbances and then simulating trajectories of the system is insufficient for approximating reach sets because all possible states of the system are not accounted for in such simulations. For this reason, analytical formulations of over-approximations $\widehat{\mathcal{X}}$ to these reach sets $\mathcal{X}$ are sought, so that $\widehat{\mathcal{X}} \supseteq \mathcal{X}$ is guaranteed via analysis. The objective of this thesis is to develop an algorithm for fast computation of $\widehat{X}$ for a given dynamical system and set-valued uncertainty descriptions.

1.2 State of the Art

Two representations for the over-approximation $\widehat{X}$ are possible: parametric and non-parametric; these lead to two distinct strands of literature. The predominant approach for non-parametric approximation for the reach set is the so-called level set method, capable of yielding exact representations of the reach sets of nonlinear systems by solving the Hamilton-Jacobi-Bellman (HJB) partial differential equation (PDE). The forward reach set of a system is solved as the set of states $\boldsymbol{x}$ that yield the sub-zero-level set of a value function $\boldsymbol{V}_0(\boldsymbol{x})$ that solves the HJB equation, $\mathcal{X}[t] = \{\boldsymbol{x} \mid \boldsymbol{V}_0(\boldsymbol{x}) \leq \boldsymbol{0}\}$ [13, p. 54]. This approach is restricted for real-time computation of the reach sets for high-dimensional systems because it suffers from the *curse of dimensionality* [3], its computational cost scales exponentially with the dimension of the state vector [16]. To address the intractability of this approach for high dimensions, the problem can be decomposed into several computations over small numbers of dimensions [7][8].

In the parametric approach, parametric descriptions of the sets are evolved in a way to provably over-approximate the reach sets. Possible convex shapes include polytopes and ellipsoids. The faces of polytopes can be described by matrices and vectors, but the number of faces cannot be fixed as the shape evolves under the system dynamics and may grow fast depending on the dynamics [14]. Thus, the main difficulty with polytopic outer-approximation is that it leads to variable-complexity computation. In contrast, the ellipsoidal parameterization adopted in this work is

a fixed-complexity computation. This is because an arbitrary ellipsoid in $\mathbb{R}^n$ can be parameterized by $n(n+3)/2$ reals, of which n reals specify its center, and the rest $n(n+1)/2$ reals specify its shape given by a symmetric positive definite matrix. Ellipsoidal representation is favorable over Euclidean n-balls because the n principal semi-axes of the ellipsoid allow a less conservative estimate of the actual reach set, whereas the radius of a bounding ball would necessarily be the maximum of these semi-axes.

Guaranteeing that the ellipsoids outwardly-bound the reach sets generated by a set-valued uncertain system is nontrivial. Even if these sets are bounded by ellipsoids, their shapes are deformed by the dynamics. Kurzhanski and Varaiya [13] developed a parametrized ordinary differential equation (ODE) describing the evolution of ellipsoids that are guaranteed to over-approximate the reach set of an LTV system. At any time t, the ODE has infinite solutions that are ellipsoids guaranteed to outwardly-bound the actual reach set $\mathcal{X}[t]$. One shortcoming of this parameterization is that the quality of the ellipsoidal approximation with respect to the initial parameter is unpredictable. Because all ellipsoids generated by "Kurzhanski's method" for a time t contain the actual reach set $\mathcal{X}[t]$, the intersection of any number of these ellipsoids must also contain the reach set. Therefore, we can take $\widehat{\mathcal{X}}[t]$ as the intersection of these parameterized ellipsoids at time t. Since the intersection of convex sets is convex, we thus get a convex over-approximation $\widehat{\mathcal{X}}[t] \supseteq \mathcal{X}[t]$ at any time t. In other words, the reach set over-approximation problem is reduced to computing the intersection of ellipsoids.

1.3 Novel Contributions

The discussion above motivates computing an over-approximation of the intersection of a parameterized family of ellipsoids. Since we want such an over-approximation to be "tight", we are naturally led to the Löwner-John optimization problem [4], which enables the calculation of $\mathcal{E}_{\mathrm{LJ}}$, a volume-minimizing ellipsoidal bound for a given convex set. Once the *minimum-volume outer-ellipsoid* (MVOE) of the intersection is computed, a simple approximation of the reachable set $\widetilde{\mathcal{X}}$ can be obtained by computing the Löwner-John MVOE of the union of the MVOEs that over-approximate the reach sets.

The algorithm that results from the implementation of the methods described above lends itself well to parallelization since computation of ellipsoidal approximations that solve Kurzhanski's ODE can be done independently and because the optimization to determine the MVOE of the reach set at each time is independent of the same at any other time.

2

Ellipsoidal Calculus for Linear Dynamical Systems

2.1 Ellipsoids

An ellipsoid in n dimensions, denoted as $\mathcal{E}(\boldsymbol{q}, \boldsymbol{Q})$, can be described as the sub-level set of a quadratic function, codified by a unique vector-matrix tuple $(\boldsymbol{q}, \boldsymbol{Q})$ where $\boldsymbol{q} \in \mathbb{R}^n$ and $\boldsymbol{Q} \in \mathbb{S}^n_+$, the cone of symmetric positive definite matrices of size $n \times n$. Symbolically, we write

$$\mathcal{E}(\boldsymbol{q}, \boldsymbol{Q}) = \{\boldsymbol{x} \in \mathbb{R}^n \mid (\boldsymbol{x} - \boldsymbol{q})^\top \boldsymbol{Q}^{-1} (\boldsymbol{x} - \boldsymbol{q}) \leq 1\}. \tag{2.1}$$

Hereafter we refer to $\boldsymbol{q}$ as the "center vector" and $\boldsymbol{Q}$ as the "shape matrix".

Lengths of the semi-axes of such an ellipsoid are the squares of the eigenvalues of

$\boldsymbol{Q}$. The volume of the ellipsoid is

$$\operatorname{vol}\left(\mathcal{E}(\boldsymbol{q}, \boldsymbol{Q})\right) = \frac{\operatorname{vol}\left(\mathcal{B}_1^n\right)}{\sqrt{\det\left(\boldsymbol{Q}^{-1}\right)}} = \frac{\pi^{\frac{n}{2}}}{\Gamma\left(\frac{n}{2}+1\right)}\sqrt{\det\left(\boldsymbol{Q}\right)}, \tag{2.2}$$

where Γ is the gamma function and $\mathcal{B}_1^n$ is the Euclidean unit n-ball [9].

Eqn. (2.1) is referred to here as the "$\boldsymbol{Qq}$" representation. There are several other parametric representations for ellipsoids, one of which, the "$\boldsymbol{Ab}c$" form, will be useful for the proposed ellipsoidal algorithm. In the "$\boldsymbol{Ab}c$", form the ellipsoid is described as

$$\mathcal{E}(\boldsymbol{A}, \boldsymbol{b}, c) = \{\boldsymbol{x} \in \mathbb{R}^n \mid \boldsymbol{x}^\top \boldsymbol{A}\boldsymbol{x} + 2\boldsymbol{x}^\top \boldsymbol{b} + c \leq 0\}, \tag{2.3}$$

where $\boldsymbol{A} \in \mathbb{S}^n$ and $\boldsymbol{b}^\top \boldsymbol{A}^{-1}\boldsymbol{b} - c > 0$. The latter requirement ensures that the ellipsoid is non-empty. Notice that $\mathcal{E}$ remains unchanged when $\boldsymbol{A}$, $\boldsymbol{b}$, and c are multiplied by any positive scalar.

The transformation from the $\boldsymbol{Qq}$ form to the $\boldsymbol{Ab}c$ form is

$$\boldsymbol{A} = \boldsymbol{Q}^{-1}, \qquad \boldsymbol{b} = -\boldsymbol{Q}^{-1}\boldsymbol{q}, \qquad c = \boldsymbol{q}^\top \boldsymbol{Q}^{-1}\boldsymbol{q} - 1, \tag{2.4}$$

and the inverse of this transformation is

$$\boldsymbol{Q} = \boldsymbol{A}^{-1}, \qquad \boldsymbol{q} = -\boldsymbol{A}^{-1}\boldsymbol{b}. \tag{2.5}$$

The affine transformation of an ellipsoid is another ellipsoid. To verify this, let $\boldsymbol{y} \coloneqq \boldsymbol{C}\boldsymbol{x} + \boldsymbol{d}$ so that $\boldsymbol{x} = \boldsymbol{C}^{-1}(\boldsymbol{y} - \boldsymbol{d})$, where $\boldsymbol{C} \in \mathbb{R}^{n\times n}$ is invertible and $\boldsymbol{d} \in \mathbb{R}^n$.

Then the condition in Eqn. (2.1) becomes

$$\begin{aligned} 1 &\geq \left(\boldsymbol{C}^{-1}(\boldsymbol{y}-\boldsymbol{d})-\boldsymbol{q}\right)^{\top}\boldsymbol{Q}^{-1}\left(\boldsymbol{C}^{-1}(\boldsymbol{y}-\boldsymbol{d})-\boldsymbol{q}\right) \\ &= \left(\boldsymbol{C}^{-1}(\boldsymbol{y}-\boldsymbol{d}-\boldsymbol{C}\boldsymbol{q})\right)^{\top}\boldsymbol{Q}^{-1}\left(\boldsymbol{C}^{-1}(\boldsymbol{y}-\boldsymbol{d}-\boldsymbol{C}\boldsymbol{q})\right) \\ &= (\boldsymbol{y}-(\boldsymbol{C}\boldsymbol{q}+\boldsymbol{d}))^{\top}\left(\boldsymbol{C}\boldsymbol{Q}\boldsymbol{C}^{\top}\right)^{-1}(\boldsymbol{y}-(\boldsymbol{C}\boldsymbol{q}+\boldsymbol{d}))\,. \end{aligned} \tag{2.6}$$

Comparing the last line with Eqn. (2.1), it is evident that under affine transformation $\boldsymbol{y}=\boldsymbol{C}\boldsymbol{x}+\boldsymbol{d}$ the ellipsoid $\mathcal{E}(\boldsymbol{q},\boldsymbol{Q})$ becomes the ellipsoid $\mathcal{E}(\boldsymbol{C}\boldsymbol{q}+\boldsymbol{d},\boldsymbol{C}\boldsymbol{Q}\boldsymbol{C}^{\top})$.

A non-empty, closed, convex set $\mathcal{X}\subset\mathbb{R}^n$ can be uniquely described by its support function [13, p. 20],

$$\rho(\boldsymbol{\ell}|\mathcal{X}) = \max\{\langle\boldsymbol{\ell},\boldsymbol{x}\rangle \mid \boldsymbol{x}\in\mathcal{X}\}, \tag{2.7}$$

where $\langle\cdot,\cdot\rangle$ denotes the Euclidean inner product. Therefore, the function $\rho:\mathcal{X}\mapsto\mathbb{R}$. We clarify here that the maximization in (2.7) is over all vectors $\boldsymbol{x}\in\mathcal{X}$. If the non-empty, closed convex set $\mathcal{X}$ is also bounded then the support function returns finite scalars. The function $\rho\left(\boldsymbol{\ell}|\mathcal{X}\right)$ is convex in the vector variable $\boldsymbol{\ell}\in\mathbb{R}^n$, and encodes the distances from the origin to the supporting hyperplanes of $\mathcal{X}$. The support function of an ellipsoidal set $\mathcal{E}(\boldsymbol{q},\boldsymbol{Q})$ is given by [13, p. 89]

$$\rho(\boldsymbol{\ell}|\mathcal{E}(\boldsymbol{q},\boldsymbol{Q})) = \max\{\langle\boldsymbol{\ell},\boldsymbol{x}\rangle \mid \boldsymbol{x}\in\mathcal{E}(\boldsymbol{q},\boldsymbol{Q})\} \tag{2.8}$$

$$= \langle\boldsymbol{\ell},\boldsymbol{q}\rangle \ + \langle\boldsymbol{\ell},\boldsymbol{Q}\boldsymbol{\ell}\rangle^{1/2}. \tag{2.9}$$

2.2 Linear Time-Varying Dynamical Systems

We consider the linear time-varying (LTV) dynamical system in continuous-time, given by

$$\dot{\boldsymbol{x}}(t) = \boldsymbol{A}(t)\,\boldsymbol{x}(t) + \boldsymbol{B}(t)\,\boldsymbol{u}(t) + \boldsymbol{G}(t)\,\boldsymbol{w}(t) \tag{2.10}$$

where the state $\boldsymbol{x}(t) \in \mathbb{R}^n$, the controls $\boldsymbol{u}(t) \in \mathbb{R}^m$, the exogenous disturbances $\boldsymbol{w}(t) \in \mathbb{R}^d$, $\boldsymbol{A}(t) \in \mathbb{R}^{n\times n}$, $\boldsymbol{B}(t) \in \mathbb{R}^{n\times m}$, and $\boldsymbol{G}(t) \in \mathbb{R}^{n\times d}$ for all $t \in [t_0, \infty)$. We consider the control $\boldsymbol{u}(x,t) \coloneqq \boldsymbol{u}_{\text{feedback}}(x,t) + \boldsymbol{u}_{\text{feedforward}}(t)$. Furthermore, we assume linear state feedback, i.e., $\boldsymbol{u}_{\text{feedback}}(x,t) \coloneqq \boldsymbol{K}(t)\boldsymbol{x}(t)$ and let $\boldsymbol{u}_{\text{feedforward}}(t) \equiv \boldsymbol{v}(t)$. Then we can rewrite Eqn. (2.10) as

$$\dot{\boldsymbol{x}}(t) = \boldsymbol{A}_{\text{cl}}(t)\,\boldsymbol{x}(t) + \boldsymbol{B}(t)\,\boldsymbol{v}(t) + \boldsymbol{G}(t)\,\boldsymbol{w}(t), \tag{2.11}$$

with $\boldsymbol{A}_{\text{cl}}(t) \coloneqq \boldsymbol{A}(t) + \boldsymbol{B}(t)\boldsymbol{K}(t)$ where $\boldsymbol{K}(t) \in \mathbb{R}^{m\times n}$ denotes the feedback gain matrix at time t. We will consider the evolution of set-valued uncertainties subject to the LTV dynamics (2.10) or (2.11).

2.3 Evolving Ellipsoids with LTV Dynamics

We model the set-valued uncertainties in initial states, controls, and exogenous disturbances in (2.10) as non-degenerate ellipsoids given by

$$\begin{aligned} \boldsymbol{x}(t_0) &\in \mathcal{E}\left(\boldsymbol{x}_0, \boldsymbol{X}_0\right), \\ \boldsymbol{u}(t) &\in \mathcal{E}\left(\boldsymbol{u}_{\text{c}}(t), \boldsymbol{U}(t)\right), \\ \boldsymbol{w}(t) &\in \mathcal{E}\left(\boldsymbol{w}_{\text{c}}(t), \boldsymbol{W}(t)\right), \end{aligned} \tag{2.12}$$

where the center vectors $\boldsymbol{x}_0 \in \mathbb{R}^n$, $\boldsymbol{u}_{\mathrm{c}}(t) \in \mathbb{R}^m$, $\boldsymbol{w}_{\mathrm{c}}(t) \in \mathbb{R}^d$ for all $t \geq t_0$. Furthermore, the shape matrices $\boldsymbol{X}_0 \in \mathbb{S}_+^n$, $\boldsymbol{U}(t) \in \mathbb{S}_+^m$, and $\boldsymbol{W}(t) \in \mathbb{S}_+^d$ for all $t \geq t_0$. The set-valued descriptions given by Eqn. (2.12) model structured, weighted, norm-bounded uncertainties in the initial condition, controls, and disturbances.

The linear differential inclusion associated with Eqns. (2.10) and (2.12) is

$$\dot{\boldsymbol{x}}(t) \in \boldsymbol{A}(t)\mathcal{E}\left(\boldsymbol{x}_c(t), \boldsymbol{X}(t)\right) \dot{+} \boldsymbol{B}(t)\mathcal{E}\left(\boldsymbol{u}_{\mathrm{c}}(t), \boldsymbol{U}(t)\right) \dot{+} \boldsymbol{G}(t)\mathcal{E}\left(\boldsymbol{w}_{\mathrm{c}}(t), \boldsymbol{W}(t)\right) \tag{2.13}$$

where $\dot{+}$ denotes the geometric or *Minkowski sum* of sets [6], defined for arbitrary sets $\mathcal{A}, \mathcal{B} \subset \mathbb{R}^n$ as

$$\mathcal{A} \dot{+} \mathcal{B} = \{\boldsymbol{a} + \boldsymbol{b} : \boldsymbol{a} \in \mathcal{A},\ \boldsymbol{b} \in \mathcal{B}\}. \tag{2.14}$$

2.3.1 Without Controls or Disturbances

For a system without controls or disturbances ($\boldsymbol{B}(t) \equiv \boldsymbol{G}(t) \equiv 0$), the state dynamics becomes

$$\dot{\boldsymbol{x}}(t) = \boldsymbol{A}(t)\boldsymbol{x}(t), \tag{2.15}$$

which results the solution

$$\boldsymbol{x}(t) = \boldsymbol{\Phi}(t, t_0)\boldsymbol{x}_0, \tag{2.16}$$

where $\boldsymbol{\Phi}(t, t_0)$ is the state-transition matrix corresponding to the coefficient matrix $\boldsymbol{A}(t)$. Then, the reach set from an ellipsoidal initial state $\mathcal{E}(\boldsymbol{x}_0, \boldsymbol{X}_0)$ *is* itself an ellipsoid $\mathcal{E}(\boldsymbol{x}_c(t), \boldsymbol{X}(t))$ with its center $\boldsymbol{x}_c(t) = \boldsymbol{\Phi}(t, t_0)\boldsymbol{x}_0$, and its shape matrix obtained from the ODE,

$$\dot{\boldsymbol{X}}(t) = \boldsymbol{A}(t)\boldsymbol{X}(t) + \boldsymbol{X}(t)\boldsymbol{A}^{\top}(t). \tag{2.17}$$

The linear matrix differential equation (2.17) is well-known as the Lyapunov differential equation, and admits solution

$$\boldsymbol{X}(t) = \boldsymbol{\Phi}(t, t_0)\boldsymbol{X}_0\boldsymbol{\Phi}^\top(t, t_0), \tag{2.18}$$

that is, the shape matrix at any time is the congruence transformation of the initial shape matrix, and hence guaranteed to be in $\mathbb{S}^n_+$. This fact can be checked by directly substituting (2.18) in (2.17), and using the following properties of the state transition matrix $\boldsymbol{\Phi}(t, t_0)$:

$$\begin{aligned} \dot{\boldsymbol{\Phi}}(t, t_0) &= \boldsymbol{A}(t)\boldsymbol{\Phi}(t, t_0), \\ \boldsymbol{\Phi}(t_2, t_0) &= \boldsymbol{\Phi}(t_2, t_1)\boldsymbol{\Phi}(t_1, t_0), \\ \boldsymbol{\Phi}(t, t_0) &= \boldsymbol{\Phi}^{-1}(t_0, t). \end{aligned} \tag{2.19}$$

If the system is time-invariant, i.e., $\boldsymbol{A}(t)$ is constant in time, then $\boldsymbol{\Phi}(t, t_0) = e^{\boldsymbol{A}(t-t_0)}$ and the reach set is

$$\mathcal{X}[t] = \mathcal{E}\left(e^{\boldsymbol{A}(t-t_0)}\boldsymbol{x}_0,\ e^{\boldsymbol{A}(t-t_0)}\boldsymbol{X}_0 e^{\boldsymbol{A}^\top(t-t_0)}\right). \tag{2.20}$$

2.3.2 With Controls but No Disturbances

A system with controls but no disturbances ($\boldsymbol{G}(t) \equiv 0$) has reach sets given by the Minkowski sum of the transformation matrix operating on the initial set and a set-valued, *Aumann integral* [1],

$$\mathcal{X}(t, t_0, \mathcal{E}(\boldsymbol{x}_0, \boldsymbol{X}_0)) = \boldsymbol{\Phi}(t, t_0)\mathcal{X}_0 \dot{+} \int_{t_0}^{t} \boldsymbol{\Phi}(t, \tau)\boldsymbol{B}(\tau)\mathcal{U}(\tau)\ \mathrm{d}\tau. \tag{2.21}$$

Eqn. (2.21) can be equivalently described as

$$\mathcal{X}(t, t_0, \mathcal{X}_0) = \boldsymbol{x}_c(t) \dot{+} \boldsymbol{\Phi}(t, t_0)\mathcal{E}(0, \boldsymbol{X}_0) \dot{+} \int_{t_0}^{t} \boldsymbol{\Phi}(t, \tau)\mathcal{E}\left(0, \boldsymbol{B}(\tau)\boldsymbol{U}(\tau)\boldsymbol{B}^\top(\tau)\right)\, \mathrm{d}\tau \quad (2.22)$$

with the center vector guided by the Eqn. (2.10),

$$\boldsymbol{x}_c(t) = \boldsymbol{\Phi}(t, t_0)\boldsymbol{x}_0 + \int_{t_0}^{t} \boldsymbol{\Phi}(t, \tau)\boldsymbol{B}(\tau)\boldsymbol{u}_c(\tau)\, \mathrm{d}\tau. \quad (2.23)$$

The Minkowski sum of the sets in (2.21) is convex but is non-ellipsoidal in general and difficult to evaluate numerically. The support function of the Minkowski sum of two convex sets, however, is simply the sum of their support functions [13],

$$\rho(\boldsymbol{\ell}, \mathcal{A} \dot{+} \mathcal{B}) = \rho(\boldsymbol{\ell}, \mathcal{A}) + \rho(\boldsymbol{\ell}, \mathcal{B}). \quad (2.24)$$

Thus, to circumvent evaluation of the Aumann integral and Minkowski sums in Eqn. (2.21), we consider the support function of $\mathcal{X}[t]$,

$$\rho(\boldsymbol{\ell}|\mathcal{X}[t]) = \langle \boldsymbol{\ell}, \boldsymbol{x}_c \rangle + \langle \boldsymbol{\ell}, \boldsymbol{\Phi}(t, t_0)\boldsymbol{X}_0\boldsymbol{\Phi}^\top(t, t_0)\boldsymbol{\ell} \rangle^{1/2} + \int_{t_0}^{t} \langle \boldsymbol{\ell}, \boldsymbol{\Phi}(t, \tau)\boldsymbol{B}(\tau)\boldsymbol{U}(\tau)\boldsymbol{B}^\top(\tau)\boldsymbol{\Phi}^\top(t, \tau)\boldsymbol{\ell} \rangle^{1/2}\, \mathrm{d}\tau \quad (2.25)$$

which describes a convex compact set that evolves continuously as a function of t. We can consider outer ellipsoidal approximations, $\mathcal{E}_+ \supseteq \mathcal{X}[t]$ that are guaranteed to be "tight" bounds of the actual reach set if there exists an $\boldsymbol{\ell} \in \mathbb{R}^n$ such that

$$\rho(\pm\boldsymbol{\ell}|\mathcal{E}_+) = \rho(\pm\boldsymbol{\ell}|\mathcal{X}[t]). \quad (2.26)$$

This condition does not produce a unique ellipsoid, but rather a class of outer ellipsoids, parameterized by the support vectors $\boldsymbol{\ell}_i$, indexed by i, that are tight around

the reach set [13, p. 91]. Kurzhanski and Varaiya showed that the shape matrices of ellipsoidal outer-approximations of the reach sets described by Eqn. (2.25) with condition (2.26) can be recursively determined as the solutions of the ODE [13, p. 89]

$$\dot{\boldsymbol{X}}_{\boldsymbol{\ell}_i(t)}(t) = \boldsymbol{A}(t)\boldsymbol{X}_{\boldsymbol{\ell}_i(t)}(t) + \boldsymbol{X}_{\boldsymbol{\ell}_i(t)}(t)\boldsymbol{A}^\top(t) + \pi_{\boldsymbol{\ell}_i(t)}\boldsymbol{X}_{\boldsymbol{\ell}_i(t)}(t) + \frac{1}{\pi_{\boldsymbol{\ell}_i(t)}}\boldsymbol{B}(t)\boldsymbol{U}(t)\boldsymbol{B}^\top(t) \tag{2.27}$$

where $\boldsymbol{\ell}_i(t)$ is governed by the adjoint ODE

$$\dot{\boldsymbol{\ell}}_i(t) = -\boldsymbol{A}^\top(t)\boldsymbol{\ell}_i(t), \quad \boldsymbol{\ell}_{i0} = \boldsymbol{\ell}_i(t_0), \quad \langle \boldsymbol{\ell}_{i0}, \boldsymbol{\ell}_{i0} \rangle = 1, \tag{2.28}$$

and can be solved as $\boldsymbol{\ell}_i(t) = \boldsymbol{\Phi}(t, t_0)\boldsymbol{\ell}_{i0}$. The scalar function $\pi_{\boldsymbol{\ell}_i(t)}(t)$ is given by

$$\pi_{\boldsymbol{\ell}_i(t)}(t) \coloneqq \left(\frac{\boldsymbol{\ell}_i^\top(t)\boldsymbol{B}(t)\boldsymbol{U}(t)\boldsymbol{B}^\top(t)\boldsymbol{\ell}_i(t)}{\boldsymbol{\ell}_i^\top(t)\boldsymbol{X}_{\boldsymbol{\ell}_i(t)}(t)\boldsymbol{\ell}_i(t)} \right)^{1/2}. \tag{2.29}$$

2.3.3 With Controls and Disturbances

With both controls and disturbances present, the reach set generated by (2.10) and (2.12) is

$$\mathcal{X}(t, t_0, \mathcal{E}(\boldsymbol{x}_0, \boldsymbol{X}_0)) = \boldsymbol{\Phi}(t, t_0)\mathcal{X}_0 \dot{+} \int_{t_0}^{t} \boldsymbol{\Phi}(t, \tau)\big(\boldsymbol{B}(\tau)\mathcal{U}(\tau) \dot{+} \boldsymbol{G}(\tau)\mathcal{W}(\tau)\big)\, \mathrm{d}\tau. \tag{2.30}$$

Kurzhanksi and Varaiya [14, p. 20] showed that the shape matrices for tight ellipsoidal outer-approximations of the reach set given by (2.30) are solutions of the ODE

$$\begin{aligned} \dot{\boldsymbol{X}}_{\boldsymbol{\ell}_i(t)}(t) = {} & \boldsymbol{A}(t)\boldsymbol{X}_{\boldsymbol{\ell}_i(t)}(t) + \boldsymbol{X}_{\boldsymbol{\ell}_i(t)}(t)\boldsymbol{A}^\top(t) + \pi_{\boldsymbol{\ell}_i(t)}\boldsymbol{X}_{\boldsymbol{\ell}_i(t)}(t) \\ & + \frac{1}{\pi_{\boldsymbol{\ell}_i(t)}}\boldsymbol{B}(t)\boldsymbol{U}(t)\boldsymbol{B}^\top(t) - \sqrt{\boldsymbol{X}_{\boldsymbol{\ell}_i(t)}(t)}\boldsymbol{S}_{\boldsymbol{\ell}_i(t)}(t)\sqrt{\boldsymbol{G}(t)\boldsymbol{W}(t)\boldsymbol{G}^\top(t)} \\ & - \sqrt{\boldsymbol{G}(t)\boldsymbol{W}(t)\boldsymbol{G}^\top(t)}\boldsymbol{S}_{\boldsymbol{\ell}_i(t)}^\top(t)\sqrt{\boldsymbol{X}_{\boldsymbol{\ell}_i(t)}(t)} \end{aligned} \tag{2.31}$$

where $\boldsymbol{\ell}_i(t)$ and $\pi_{\boldsymbol{\ell}_{i(t)}}(t)$ are defined as in (2.28) and (2.29) and the orthogonal $n \times n$ matrix $\boldsymbol{S}_{\boldsymbol{\ell}_{i(t)}}(t)$ satisfies the scaling condition

$$\boldsymbol{S}_{\boldsymbol{\ell}_{i(t)}}(t)\frac{\sqrt{\boldsymbol{G}(t)\boldsymbol{W}(t)\boldsymbol{G}^\top(t)}\boldsymbol{\ell}_i(t)}{\left\|\sqrt{\boldsymbol{G}(t)\boldsymbol{W}\boldsymbol{G}^\top(t)}\boldsymbol{\ell}_i(t)\right\|_2} = \frac{\sqrt{\boldsymbol{X}_{\boldsymbol{\ell}_{i(t)}}(t)}\boldsymbol{\ell}_i(t)}{\left\|\sqrt{\boldsymbol{X}_{\boldsymbol{\ell}_{i(t)}}(t)}\boldsymbol{\ell}_i(t)\right\|_2}. \tag{2.32}$$

This matrix $\boldsymbol{S} \coloneqq \boldsymbol{S}_{\boldsymbol{\ell}_{i(t)}}(t)$ can be generated in $\mathrm{O}(n^2)$ runtime with the following procedure [13, p. 193],

$$\begin{gathered}
\boldsymbol{S} = \boldsymbol{I}_n + \boldsymbol{Q}_1(\boldsymbol{S}_o - \boldsymbol{I}_2)\boldsymbol{Q}_1^\top, \\
\boldsymbol{S}_o = \begin{bmatrix} c & s \\ -s & c \end{bmatrix}, \;\; c = \hat{\boldsymbol{v}}_1^\top \hat{\boldsymbol{v}}_2, \;\; s = \sqrt{1-c^2}, \;\; \hat{\boldsymbol{v}}_i = \frac{\boldsymbol{v}_i}{\|\boldsymbol{v}_i\|}, \\
\boldsymbol{Q}_1 = [\boldsymbol{q}_1, \boldsymbol{q}_2] \in \mathbb{R}^{n\times 2}, \;\; \boldsymbol{q}_1 = \hat{\boldsymbol{v}}_1, \;\; \boldsymbol{q}_2 = \begin{cases} s^{-1}(\hat{\boldsymbol{v}}_2 - c\hat{\boldsymbol{v}}_1), & s \neq 0, \\ 0, & s = 0 \end{cases},
\end{gathered} \tag{2.33}$$

where $\boldsymbol{I}_m$ is the $m \times m$ identity matrix and $\hat{\boldsymbol{v}}_1$ and $\hat{\boldsymbol{v}}_2$ are defined to be the corresponding terms in Eqn. (2.32) so that

$$\boldsymbol{S}_{\boldsymbol{\ell}_{i(t)}}(t)\hat{\boldsymbol{v}}_1 = \hat{\boldsymbol{v}}_2. \tag{2.34}$$

The ellipsoids thus generated with Kurzhanski's parameterization satisfy the asymptotic consistency condition

$$\mathcal{X}(t, t_0, \mathcal{E}(\boldsymbol{x}_0, \boldsymbol{X}_0)) = \bigcap_{i=1}^{\infty} \mathcal{E}(\boldsymbol{x}_c(t), \boldsymbol{X}_{\boldsymbol{\ell}_{i(t)}}(t)). \tag{2.35}$$

Thus, the intersection of a finite number (say, N_ℓ) of these ellipsoids can serve as an outer approximant $\widehat{\mathcal{X}}[t]$ for the true reach set $\mathcal{X}[t]$, maintaining

$$\mathcal{X}(t, t_0, \mathcal{E}(\boldsymbol{x}_0, \boldsymbol{X}_0)) \subseteq \widehat{\mathcal{X}}_{\{\boldsymbol{\ell}_{i0}\}_{i=1}^{N_\ell}}(t, t_0, \mathcal{E}(\boldsymbol{x}_0, \boldsymbol{X}_0)) = \bigcap_{i=1}^{N_\ell} \mathcal{E}\left(\boldsymbol{x}_c(t), \boldsymbol{X}_{\boldsymbol{\ell}_{i(t)}}(t)\right). \tag{2.36}$$

2.4 Löwner-John Optimization

The Löwner-John ellipsoid $\mathcal{E}_{\mathrm{LJ}}$ of a compact set is the minimum volume outer ellipsoid (MVOE) that bounds the set [10][11]. An ellipsoid described as the affine transformation of the unit ball,

$$\mathcal{E} = \{\boldsymbol{x} \in \mathbb{R}^n \mid \|\boldsymbol{A}\boldsymbol{x} + \boldsymbol{b}\|_2 \leq 1\}, \tag{2.37}$$

with $\boldsymbol{A} \in \mathrm{GL}(n)$, the general linear group of degree n (the set of invertible $n \times n$ matrices), and $\boldsymbol{b} \in \mathbb{R}^n$ (not to be confused with $\boldsymbol{A}$ and $\boldsymbol{b}$ of the $\boldsymbol{A}\boldsymbol{b}c$ parameterization), has volume proportional to $\det \boldsymbol{A}^{-1}$. Computing the MVOE of a compact set $\mathcal{S}$ thus reduces to solving the optimization problem

$$\begin{aligned} \text{minimize} \quad & \log\det \boldsymbol{A}^{-1} \\ \text{subject to} \quad & \sup_{\boldsymbol{x}\in\mathcal{S}} \|\boldsymbol{A}\boldsymbol{x} + \boldsymbol{b}\|_2 \leq 1 \end{aligned} \tag{2.38}$$

for variables $\boldsymbol{A}$ and $\boldsymbol{b}$ with the constraint $\boldsymbol{A} \succ 0$ [5, p. 410]. If the set $\mathcal{S}$ is convex, then the problem (2.38) is convex in decision variables $\boldsymbol{A}$ and $\boldsymbol{b}$, and its solutions are guaranteed to exist and be unique. The argmin pair $(\boldsymbol{A}_0, \boldsymbol{b}_0)$ then defines $\mathcal{E}_{\mathrm{LJ}}$ via (2.37). One can think of $\mathcal{E}_{\mathrm{LJ}}$ as a set-valued operator that maps the given convex set $\mathcal{S}$ to its unique MVOE.

For any given convex set $\mathcal{S}$, solving (2.38), however, is non-trivial since there are an infinite number of constraints in (2.38). In other words, (2.38) is a semi-infinite programming problem. For a given convex set $\mathcal{S}$, one needs to consider if an exact semidefinite (SDP) representation of (2.38) is possible. If not, one may then consider deriving an SDP relaxation for (2.38) valid for that particular convex set $\mathcal{S}$.

2.4.1 MVOE of the Intersection of Ellipsoids

Kurzhanski's parameterization enables the reach set (2.30) to be over-approximated as the intersection of a finite number of ellipsoids generated by the parametric ODE (2.31). The intersection of a set of ellipsoids is convex, as depicted in Figure 2.1. Our objective is to compute the Löwner-John MVOE of this intersection. However, the semi-infinite programming problem (2.38) for computing $\mathcal{E}_{\mathrm{LJ}}\left(\bigcap_{i=1}^{N_\ell}\mathcal{E}_i\right)$ that contains the intersection of N_ℓ ellipsoids, i.e.,

$$\mathcal{E}_{\mathrm{LJ}} \supseteq \bigcap_{i=1}^{N_\ell} \mathcal{E}_i \tag{2.39}$$

has no known exact SDP representation. We instead focus on computing a suboptimal MVOE $\mathcal{E}_0$ that can be solved as an SDP relaxation of (2.38), that is, $\mathcal{E}_0 \supseteq \mathcal{E}_{\mathrm{LJ}}\left(\bigcap_{i=1}^{N_\ell}\mathcal{E}_i\right)$.

There exist several methods for computing suboptimal MVOEs of the intersection of some N_ℓ ellipsoids [4, p. 44]. We use the $\mathcal{S}$-procedure [18, p. 62] to derive an SDP relaxation for the same. The resulting SDP is written for ellipsoids in the $\boldsymbol{Abc}$ form, requiring the transformation given in Eqn. (2.4) to solve and the transformation in Eqn. (2.5) to obtain $\mathcal{E}_0$ in our preferred $\boldsymbol{Qq}$ form.

The $\mathcal{S}$-procedure yields the sufficient inclusion condition that there exist non-negative scalars $\tau_1 \dots \tau_{N_\ell}$ such that

$$\begin{bmatrix} \boldsymbol{A}_0 & \boldsymbol{b}_0 \\ \boldsymbol{b}_0^\top & \boldsymbol{b}_0^\top \boldsymbol{A}_0^{-1}\boldsymbol{b}_0 - 1 \end{bmatrix} - \sum_{i=1}^{N_\ell} \tau_i \begin{bmatrix} \boldsymbol{A}_i & \boldsymbol{b}_i \\ \boldsymbol{b}_i^\top & c_i \end{bmatrix} \leq 0 \tag{2.40}$$

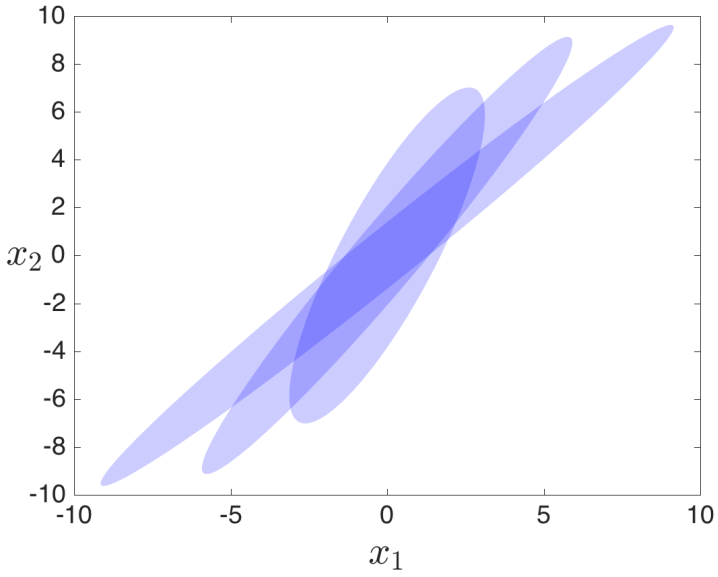

Figure 2.1: The dark shaded region is the intersection of the three ellipsoidal sets, depicted.

where $\boldsymbol{A}_0$, $\boldsymbol{b}_0$, c_0 are normalized to satisfy

$$c_0 = \boldsymbol{b}^\top \boldsymbol{A}_0^{-1} \boldsymbol{b}_0 - 1. \tag{2.41}$$

for convenience. This normalization is allowed by the homogeneity of the $\boldsymbol{Ab}c$ representation for the ellipsoid $\mathcal{E}_0$.

Eqn. (2.40) can be rewritten as the linear matrix inequality (LMI)

$$\begin{bmatrix} \boldsymbol{A}_0 & \boldsymbol{b}_0 & 0 \\ \boldsymbol{b}_0^\top & -1 & \boldsymbol{b}_0^\top \\ 0 & \boldsymbol{b}_0 & -\boldsymbol{A}_0 \end{bmatrix} - \sum_{i=1}^{N_\ell} \tau_i \begin{bmatrix} \boldsymbol{A}_i & \boldsymbol{b}_i & 0 \\ \boldsymbol{b}_i^\top & \boldsymbol{c}_i & 0 \\ 0 & 0 & 0 \end{bmatrix} \leq 0. \tag{2.42}$$

The LMI (2.42) is a sufficient condition for $\mathcal{E}_0 \supseteq \mathcal{E}_{\mathrm{LJ}}\left(\bigcap_{i=1}^{N_\ell} \mathcal{E}_i\right)$, hence the suboptimality of its solutions. The ellipsoid that satisfies (2.42) with least volume is

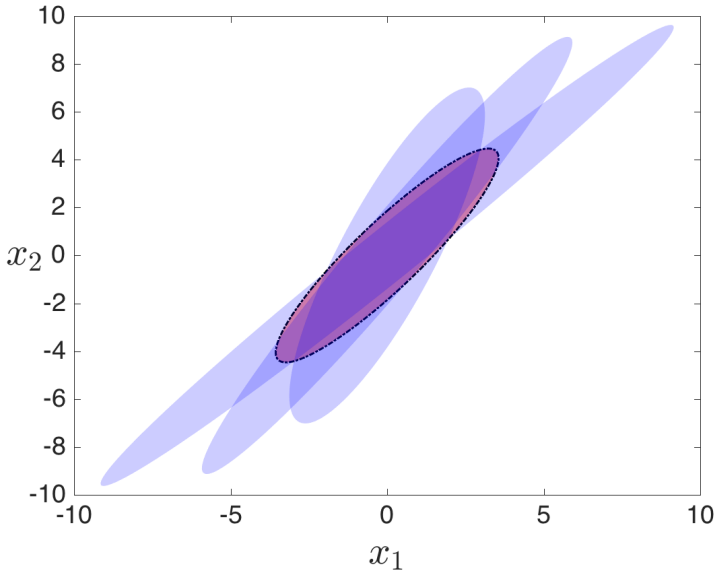

Figure 2.2: The MVOE that bounds the intersection of the three ellipses, shown in Figure 2.1, is filled in red with a dashed boundary.

determined by solving the SDP

$$\begin{aligned} \text{minimize} \quad & \log\det \boldsymbol{A}_0^{-1} \\ \text{subject to} \quad & \boldsymbol{A}_0 \succ 0, \qquad \tau_1 \geq 0, \ldots, \tau_{N_\ell} \geq 0. \end{aligned} \tag{2.43}$$

In Figure 2.2 the MVOE is the red-filled ellipse with dashed boundary that solves the problem (2.43) to outer-approximate the intersection of the blue ellipses. We summarize: the solution of the SDP (2.43) can be used to find a suboptimal Löwner-John MVOE for the intersection of the N_ℓ ellipsoids generated with the Kurzhanski parameterization that is guaranteed to be a better outer-approximation than any one of the N_ℓ ellipsoids alone.

2.4.2 MVOE of the Union of Ellipsoids

Unlike the problem of computing the MVOE for the intersection of ellipsoids, that for the union of ellipsoids is an exact SDP [5, p. 411]. Using the $\boldsymbol{Abc}$ parameterization of ellipsoids, the MVOE $\mathcal{E}_{\mathrm{LJ}}$ of the union of some N_ℓ ellipsoids is computed by solving

$$\begin{aligned} \text{minimize} \quad & \log\det \boldsymbol{A}_0^{-1} \\ \text{subject to} \quad & \boldsymbol{A}_0 \succ 0, \qquad \tau_1 \geq 0, \ldots, \tau_{N_\ell} \geq 0 \\ & \begin{bmatrix} \boldsymbol{A}^2 - \tau_i \boldsymbol{A}_i & \tilde{\boldsymbol{b}} - \tau_i \boldsymbol{b}_i & 0 \\ (\tilde{\boldsymbol{b}} - \tau_i \boldsymbol{b}_i)^\top & -1 - \tau_i c_i & \tilde{\boldsymbol{b}}^\top \\ 0 & \tilde{\boldsymbol{b}} & -A^2 \end{bmatrix} \prec 0, \quad i = 1, \ldots, N_\ell, \end{aligned} \tag{2.44}$$

where $\tilde{\boldsymbol{b}} \coloneqq \boldsymbol{Ab}$. This problem is convex in the variables $\boldsymbol{A}^2 \in \mathbb{S}^n_+$, $\tilde{\boldsymbol{b}}$, and $\tau_1, \ldots, \tau_{N_\ell}$.

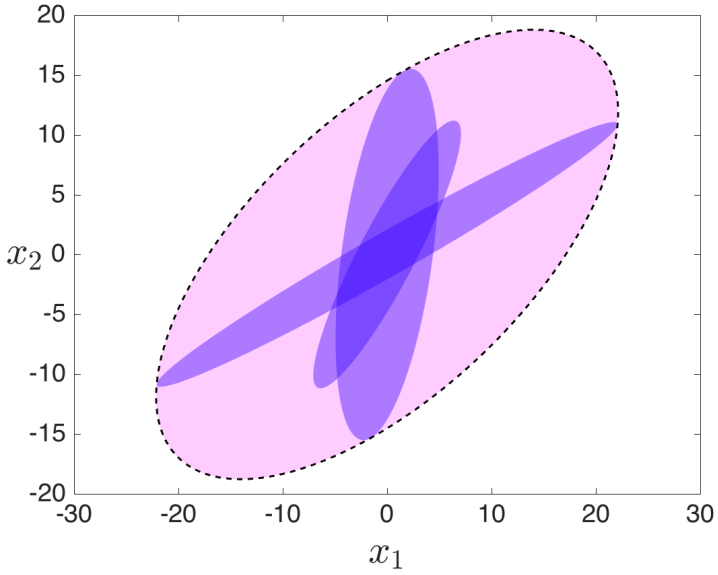

Figure 2.3: The pink ellipse with dashed boundary is the MVOE of the union of the three darker ellipses.

This procedure can be used to obtain a low-complexity parameterization of the

reachable set $\widetilde{X}$ of a system given a set of K ellipsoids that approximate the reach sets for a sequence of K discrete times. The reachable set $\widetilde{X}$ is then outer-approximated as an ellipsoidal cylinder over the time interval $[t_0,\ t_K]$ with uniform cross-section,

$$\mathcal{E}_{\mathrm{LJ}}\left(\bigcup_{k=1}^{K}\mathcal{E}\left(\boldsymbol{x}_c(t_k),\boldsymbol{X}_{\boldsymbol{\ell}_{i(t)}}(t_k)\right)\right). \tag{2.45}$$

Figure 2.3 shows the MVOE, dashed, of the union of three depicted ellipses.

2.5 Projection of Solution

Oftentimes reachable tube solutions for a subset of states are sought. For example, in vehicular collision avoidance applications, reachable tubes are typically desired for only the three spatial dimensions. In our setting, the projection of the cross section of the uniform outer-ellipsoidal approximation for the reachable tube is

$$\mathrm{proj}\left(\mathcal{E}_{\mathrm{LJ}}\left(\bigcup_{k=1}^{K}\mathcal{E}_{\mathrm{LJ}}\left(\bigcap_{i=1}^{N_\ell}\mathcal{E}\left(\boldsymbol{x}_c(t_k),\boldsymbol{X}_{\boldsymbol{\ell}_{i(t_k)}}(t_k)\right)\right)\right)\right). \tag{2.46}$$

Conveniently, we are able to commute the projection operator, dramatically reducing the computational runtime of the algorithm. On the other hand, the set union commutes with any (even nonlinear) transformation. This can be shown for a general nonlinear function f,

$$\begin{aligned} f\circ(\mathcal{A}\cup\mathcal{B}) &= f\circ\{c : c\in\mathcal{A} \text{ or } c\in\mathcal{B}\} \\ &= \{f\circ c : c\in\mathcal{A} \text{ or } c\in\mathcal{B}\} \\ &= (f\circ\mathcal{A})\cup(f\circ\mathcal{B}) \end{aligned} \tag{2.47}$$

The Löwner-John optimization also commutes with linear operators such as the projection [5, p. 415]. The intersection of sets commutes with operators only if they are injective. Since the projection operator is guaranteed to be non-injective, the projection of the intersection of the sets is a subset of the intersection of the projection of the sets [15]. With these observations in place, we can compute

$$\mathcal{E}_{\mathrm{LJ}}\left(\bigcup_{k=1}^{K}\mathcal{E}_{\mathrm{LJ}}\left(\bigcap_{i=1}^{N_\ell}\mathrm{proj}\left(\mathcal{E}\left(\boldsymbol{x}_c(t_k),\boldsymbol{X}_{\boldsymbol{\ell}_{i(t_k)}}(t_k)\right)\right)\right)\right) \tag{2.48}$$

which is a superset of the set given by Eqn. (2.46).

3

Algorithm

The proposed algorithm approximates the projected reachable tube of a given dynamical system for a specified discrete sequence of times $\mathcal{T}$ with a single outer-bounding ellipsoid that is constant along the time-axis of the tube approximation. The algorithm is outlined as follows,

Integrate Eqn. (2.10) to get $\boldsymbol{x}_c(t_k)$ for all $t_k \in \mathcal{T}$

Generate N_ℓ random unit vectors

for $i = 1$ to N_ℓ **do**

Integrate Kurzhanski's ODE (Eqn. (2.31)) to get $\boldsymbol{X}_{\boldsymbol{\ell}_i}(t_k)$ for all $t_k \in \mathcal{T}$

Project $\boldsymbol{x}_c(\mathcal{T})$ and $\boldsymbol{X}_{\boldsymbol{\ell}_i}(\mathcal{T})$ onto desired subset of space dimensions

end for

for each $t_k \in \mathcal{T}$ **do**

Solve CP (Eqn. (2.43)) to get $\mathcal{E}_{\text{LJ}}$ of intersection of N_ℓ ellipsoids at time t_k

end for

Solve SDP (Eqn. (2.44)) to get $\mathcal{E}_{\mathrm{LJ}}$ of the union of the MVOEs of the intersections

Return $\mathcal{E}_{\mathrm{LJ}}$

The processes within the for-loops are independent of each other. As a result, the loops are well-suited for parallelization. Figure 3.1 depicts algorithm's stages and its inherent parallel structure.

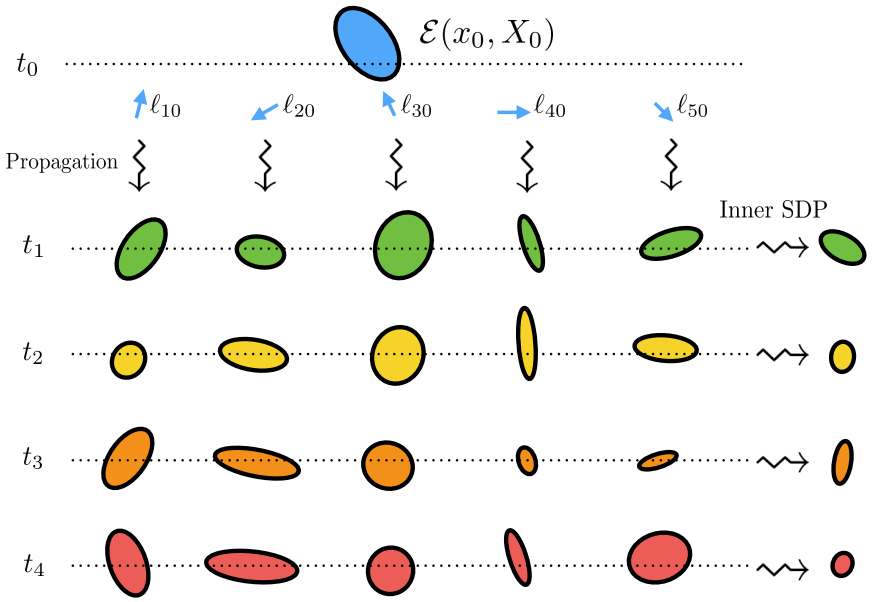

Figure 3.1: A schematic that illustrates the parallel nature of the algorithm. The vertical broken arrows denote the parallel propagation of ellipsoidal reach set estimates with Kurzhanski's ODE (2.31) for five parameterizing $\boldsymbol{\ell}_{i0}$ vectors. The horizontal broken arrows labeled "Inner SDP" are the parallelizable computations of the MVOEs for the intersections of the ellipsoids at each of the four time steps.

4

Numerical Results

4.1 Reach Sets for the Double Integrator System with Bounded Control

The double integrator, having known reach set solutions, is an ideal system to demonstrate and analyze the performance of the proposed algorithm. The two-dimensional double integrator system is the planar system $\ddot{x} = u$ with symmetrically bounded control, $|u| \leq \mu$, can be written in the state-space form,

$$\begin{gathered} \dot{x}_1 \;=\; x_2, \quad \dot{x}_2 \;=\; u, \\ x_1(0) \;=\; x_1^0, \quad x_2(0) \;=\; x_2^0; \quad |u| \leq \mu, \quad \mu > 0. \end{gathered} \tag{4.1}$$

The exact reach set for this system is known to be a compact set with two distinct boundaries: upper and lower. These two boundaries meet at two corner points (see

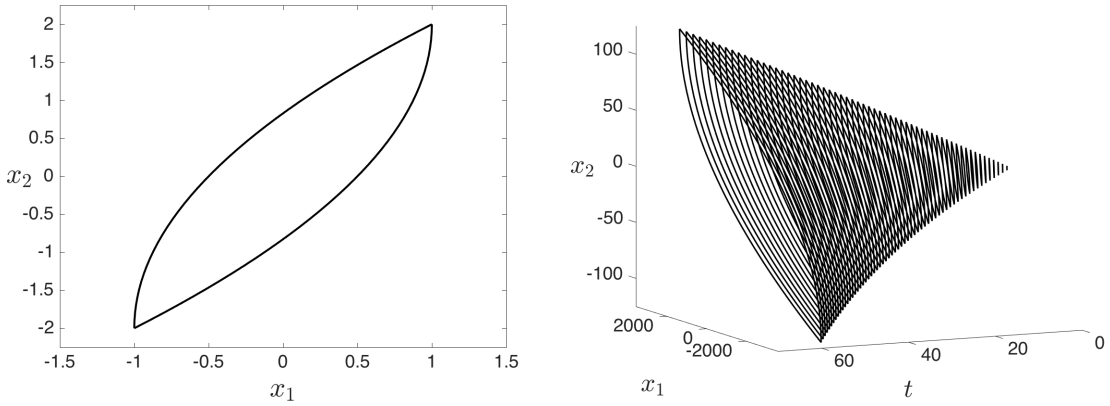

Figure 4.1: **Left:** The analytical reach set of the double integrator system at $t = 1$ with control $|u| \leq 2$ and initial state $(x_1^0, x_2^0) = (0, 0)$. **Right:** A discretization of the analytical reachable tube of the double integrator with control $|u| \leq .3$ and initial state $(x_1^0, x_2^0) = (0, 0)$. The tube describes the reachable states over $60s$, evaluated at single-second intervals.

Fig. 4.1(Left)). The parametric equation for the upper

$$x_1^+(t) = x_1^0 + x_2^0 t - \mu(t^2/2 - \sigma^2) \qquad x_2^+(t) = x_2^0 - 2\mu\sigma - \mu t \tag{4.2}$$

and the same for the lower boundary is given by

$$x_1^-(t) = x_1^0 + x_2^0 t + \mu(t^2/2 - \sigma^2), \qquad x_2^-(t) = x_2^0 + 2\mu\sigma + \mu t, \tag{4.3}$$

with the parameter σ constrained to the interval $[-t, 0]$ [13, p. 111]. A reach set defined by these curves is shown on the left in Figure 4.1. The union of these reach sets over an interval of time is the reachable set $\widetilde{\mathcal{X}}$ for the system. A wireframe plot for the three-dimensional set $\widetilde{\mathcal{X}}$ is shown on the right in Figure 4.1.

Slight reformulation of the system is necessary to approximate the reachable tube of the system with the proposed ellipsoidal algorithm. The scalar interval $|u| \leq \mu$

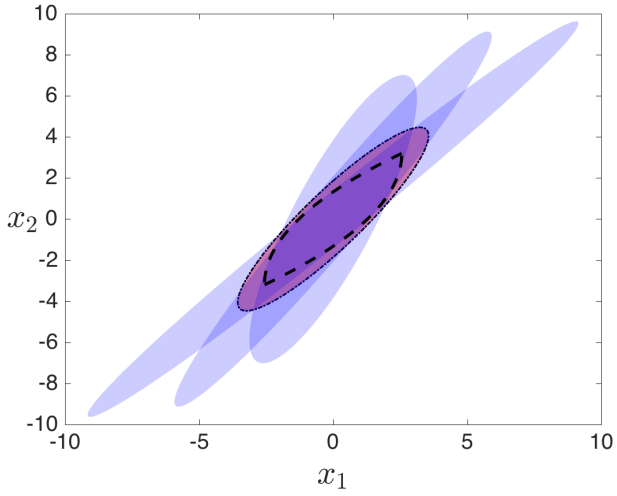

Figure 4.2: The analytical reach set (heavy dash) at $t = 1.6$ of the 2D double integrator with $|u| \leq 2$ and $\boldsymbol{x}_0 = (0, 0)$. Also pictured are outer-approximating ellipses (blue without outline) generated with Kurzhanski's parameterization, and the MVOE of the intersection of these ellipses (red-filled, thin dashed outline).

can be represented as the inclusion $u \in \mathcal{E}(0, \mu^2)$ for a one-dimensional ellipsoid in the $\boldsymbol{Qq}$ form that is centered at the origin with shape given by μ^2. To approximate a point-valued initial condition (x_1^0, x_2^0) we use a near-degenerate ellipse $\mathcal{E}(\boldsymbol{x}_0, \boldsymbol{X}_0)$ with $\boldsymbol{x}_0 = (x_1^0, x_2^0)$ and $\boldsymbol{X}_0 = \varepsilon \boldsymbol{I}$ where ε is a small scalar, 10^{-4} for this simulation, and $\boldsymbol{I}$ is the 2×2 identity matrix.

Figure 4.2 overlays ellipsoidal outer-approximations (blue with no boundary line) of the reach set of the double integrator under initial condition $(x_1^0, x_2^0) = (0, 0)$ and control constraint $|u| \leq 2$ with the known analytical solution and the MVOE that the algorithm yields (red with dashed boundary).

Figure 4.3 depicts the analytical and approximated reach sets for the double inte-

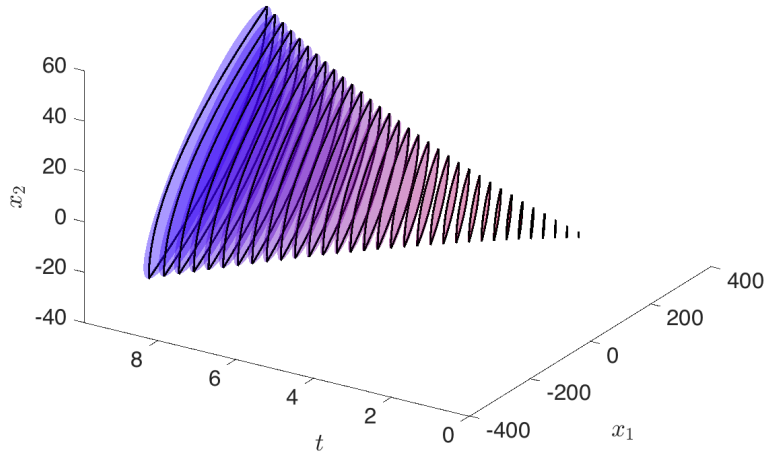

Figure 4.3: Overlaid analytical (outlined, no fill) and approximated (filled, no outline) solutions for reach sets of the double integrator (4.1).

grator at different times $t \in [0, 10]$. As designed, solutions generated by the ellipsoidal algorithm always outwardly bound the actual reach set.

For a quantitative measure of the performance of the ellipsoidal algorithm, we compare the areas of the analytical reach sets,

$$\text{area}(\mathcal{X}[t]) = 2/3\ \mu^2 t^3, \tag{4.4}$$

calculated in Appendix A, with the areas of the ellipsoidal over-approximations, calculated with Eqn. (2.2) as

$$\text{area}(\mathcal{E}(\boldsymbol{q}, \boldsymbol{Q})) = \pi\sqrt{\det(\boldsymbol{Q})}. \tag{4.5}$$

On the left of Figure 4.4 is a plot of the ratios between the areas of the actual and simulated reach sets for several reachable tube approximations, each computed

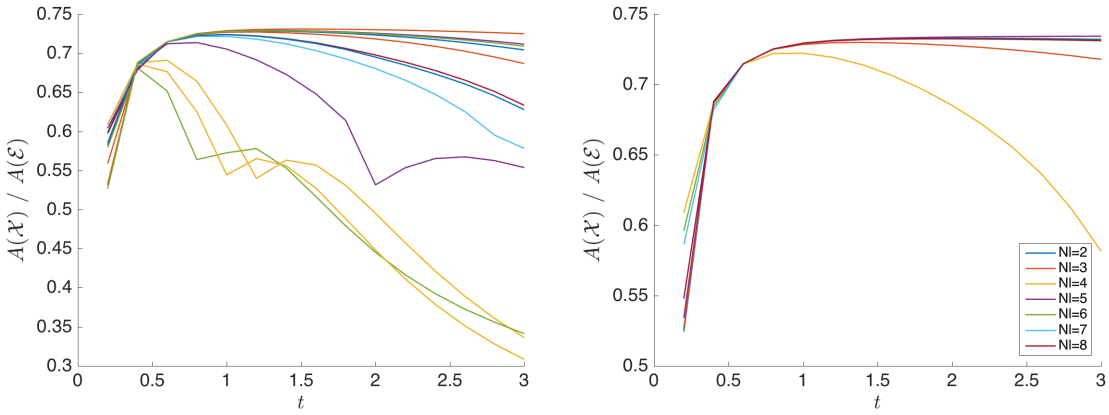

Figure 4.4: **Left:** A plot showing the ratio between the areas of analytical and numerical reach sets for the double integrator system. The 12 numerical solutions are obtained from the algorithm for $N_\ell = 3$ in order to demonstrate the variance between simulations that results from random generation of the parameterizing unit vectors, $\boldsymbol{\ell}_{i0}$. **Right:** A plot of the same where the numerical solutions are obtained from optimizations over the intersection of varying numbers ($N_\ell = 2, \ldots, 8$) of parameterized ellipsoids.

as optimizations over the intersection of $N_\ell = 3$ ellipsoids parameterized by randomly generated $\boldsymbol{\ell}_{i0}$ vectors. Because there is no ellipsoid that describes the analytical reach set we never expect that this ratio will be unity and instead look to see that the ratio is sufficiently close to one. This figure shows that there is some inconsistency in the quality of the reach set computation. The right of Figure 4.4 is a plot of the same ratios for solutions generated for varying N_ℓ. This plot confirms the hypothesis that higher N_ℓ implies better approximations.

4.2 Comparing Sequential vs. Parallel Implementation

To understand the computational benefit of parallelizing the algorithm, we compare the runtimes of the sequential and parallelized code to solve randomly generated systems over a fixed time interval. Figure 4.5 portrays the runtimes of series and parallel solutions for 15 randomly generated systems using various N_ℓ. On 2013 MacBook Pro with 2.7 GHz Intel Core i7 Processor (two cores), we see from Figure 4.5 that the the algorithm executing with parfor performs about twice as fast as the series algorithm. This confirms the hypothesis that the computation is inversely scaled with the number of threads used in the parallel computation.

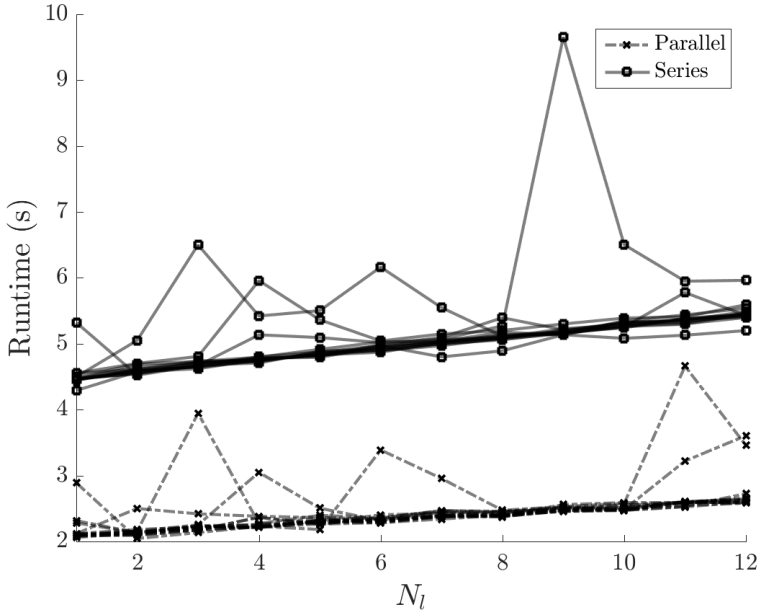

Figure 4.5: The runtimes of the parallel and sequential computations for generating the reachable tube for a $5s$ time span with reach sets computed at $.5s$ intervals. The runtimes of computations with $N_\ell = 1, \ldots, 12$ for 15 randomly simulated systems with dimensions $(n, m, d) = (12, 4, 3)$ are shown.

5

Conclusion

5.1 Summary

The ellipsoidal algorithm proposed here enables the real-time computation of reachable tubes for applications such as the safety verification of autonomous agents. The algorithm is enabled by existing ellipsoidal schemes and parallel computation and its efficacy is demonstrated by comparison with a known case: the double integrator with bounded control, and by comparison of the computation times of the reachable tubes for various systems for a variety of N_ℓ with parallel and sequential computations. These results show that the algorithm is a competitive scheme for the real-time computation of reachable sets.

5.2 Open Questions and Future Directions

To further examine the performance of the algorithm, a comparison between the runtimes of parallel computations on a processor with more than two cores would further verify the use of parallel computing and the algorithm's applicability to real-time scenarios. Additionally, the volume-minimizing algorithm proposed here may a competitive option for reach set computation that seeks to minimize some other attribute such as the trace of the ellipsoid's shape matrix. The performance of the algorithm for such objectives has yet to be investigated.

For differentially flat systems there exists an injective transformation of the system to the Brunovsky form, a generalized system of integrators in n dimensions, and an inverse transformation to do the reverse. Analytically obtained reach sets of the system of integrators can yield the reach sets of differentially flat systems by the inverse transformation that makes the flat system into that of integrators. Given that quadrotor and car dynamics are known to be differentially flat, this approach may have widespread applications.

Appendix A

Area of the Reach Set for the Double Integrator

We analytically compute the area of the reach set for the double integrator by integrating the difference between the curves (4.2) and (4.3) that bound the set. We first rewrite the equations that define the lower and upper curves, respectively, as

$$x_2^-(t) = x_2^0 + \mu t + \sqrt{\mu}\left(x_1^0 + x_2^0 t - x_1(t) - \mu t^2/2\right)^{1/2} \tag{A.1}$$

and

$$x_2^+(t) = x_2^0 - \mu t - \sqrt{\mu}\left(x_1(t) - x_1^0 - x_2^0 t - \mu t^2/2\right)^{1/2} \tag{A.2}$$

for $x_1 \in [x_\ell,\, x_r] \coloneqq [x_1^0 + x_2^0 t - \mu t^2/2,\; x_1^0 + x_2^0 t + \mu t^2/2]$. In words, the left and right endpoints of the set $\mathcal{X}[t]$ are $x_\ell \coloneqq x_1^0 + x_2^0 t - \mu t^2/2$ and $x_r \coloneqq x_1^0 + x_2^0 t + \mu t^2/2$. The

area can then be expressed as

$$\begin{aligned}\text{area}(\mathcal{X}[t]) &= \int_{x_\ell}^{x_r} x_2^+(t) - x_2^-(t)\ \mathrm{d}x_1 \\ &= -2\sqrt{\mu}t \int_{x_\ell}^{x_r} \sqrt{\mu} + \left[\left(x_1(t) - x_1^0 - x_2^0 t - \frac{\mu t^2}{2} \right)^{1/2} \right. \\ &\qquad \left. - \left(x_1^0 + x_2^0 t + x_1(t) - \frac{\mu t^2}{2} \right)^{1/2} \right] \mathrm{d}x_1. \end{aligned} \tag{A.3}$$

Integrating the first term above is straightforward and for the remaining terms, we make the substitution $y \coloneqq x_1(t) - x_1^0 - x_2^0 t$, which transforms $(x_l, x_r) \mapsto (y_l, y_r)$ where $y_\ell \coloneqq -\mu t^2/2$ and $y_r \coloneqq \mu t^2/2$. The area is then computed as

$$\begin{aligned}\text{area}(\mathcal{X}[t]) &= -2\mu t x_1 \Big|_{x_\ell}^{x_r} - 2\sqrt{\mu} \int_{y_\ell}^{y_r} \left(y - \mu t^2/2\right)^{1/2} - \left(y + \mu t^2/2\right)^{1/2}\ \mathrm{d}y \\ &= -2\mu t(\mu t^2) - 2\sqrt{\mu} \cdot \frac{2}{3} \left[(y - \mu t^2/2)^{3/2} - (y + \mu t^2/2)^{3/2} \right] \Big|_{y_\ell}^{y_r} \\ &= -2\mu^2 t^3 - \frac{4\sqrt{\mu}}{3} \left[\left(0 - \left(\mu t^2\right)^{3/2} \right) - \left(\left(\mu t^2\right)^{3/2} - 0 \right) \right] \\ &= -2\mu^2 t^3 - \frac{4\sqrt{\mu}}{3} \left(-2\mu^{3/2} t^3 \right) = -2\mu^2 t^3 + \frac{8}{3}\mu^2 t^3 = \frac{2}{3}\mu^2 t^3. \end{aligned} \tag{A.4}$$

Bibliography

[1] Robert J Aumann. Integrals of set-valued functions. *Journal of Mathematical Analysis and Applications*, 12(1):1–12, 1965.

[2] Somil Bansal, Mo Chen, Sylvia Herbert, and Claire J Tomlin. Hamilton-jacobi reachability: A brief overview and recent advances. In *Decision and Control (CDC), 2017 IEEE 56th Annual Conference on*, pages 2242–2253. IEEE, 2017.

[3] Richard Bellman. *Dynamic programming*. Courier Corporation, 2013.

[4] Stephen Boyd, Laurent El Ghaoui, Eric Feron, and Venkataramanan Balakrishnan. *Linear Matrix Inequalities in System and Control Theory*. Society for Industrial and Applied Mathematics, Philadelphia, 1994.

[5] Stephen Boyd and Lieven Vandenberghe. *Convex Optimization*. Campridge University Press, New York, 2004.

[6] Herbert Busemann. The foundations of minkowskian geometry. *Commentarii Mathematici Helvetici*, 24(1):156–187, 1950.

[7] Mo Chen, Sylvia Herbert, and Claire J Tomlin. Fast reachable set approximations

via state decoupling disturbances. In *Decision and Control (CDC), 2016 IEEE 55th Conference on*, pages 191–196. IEEE, 2016.

[8] Mo Chen, Sylvia L Herbert, Mahesh Vashishtha, Somil Bansal, and Claire J Tomlin. Decomposition of reachable sets and tubes for a class of nonlinear systems. *IEEE Transactions on Automatic Control*, 2018.

[9] Abhishek Halder. On the Parameterized Computation of Minimum Volume Outer Ellipsoid of Minkowski Sum of Ellipsoids. *ArXiv e-prints*, March 2018.

[10] Martin Henk. löwner-john ellipsoids. *Documenta Math*, pages 95–106, 2012.

[11] Fritz John. Extremum problems with inequalities as subsidiary conditions. In *Traces and emergence of nonlinear programming*, pages 197–215. Springer, 2014.

[12] Alexander Kurzhanski and István Vályi. *Ellipsoidal Calculus for Estimation and Control*. Birkhäuser Boston and International Institute for Applied Systems Analysis, 1997.

[13] Alexander B. Kurzhanski and Pravin Varaiya. *Dynamics and Control of Trajectory Tubes*. Springer International Publishing, Switzerland, 2014.

[14] Alex A Kurzhanskiy and Pravin Varaiya. Ellipsoidal toolbox (et). In *Decision and Control, 2006 45th IEEE Conference on*, pages 1498–1503. IEEE, 2006.

[15] Alexey I Kushnir and Shuo Liu. On linear transformations of intersections. 2017.

[16] Ian Mitchell and Claire J Tomlin. Level set methods for computation in hybrid systems. In *International Workshop on Hybrid Systems: Computation and Control*, pages 310–323. Springer, 2000.

[17] Ian M Mitchell. Comparing forward and backward reachability as tools for safety analysis. In *International Workshop on Hybrid Systems: Computation and Control*, pages 428–443. Springer, 2007.

[18] Lieven Vandenberghe and Stephen Boyd. Semidefinite programming. *SIAM review*, 38(1):49–95, 1996.